

Supporting Information

Hollow NiFe₂O₄ Nanospheres on Carbon Nanorods as a Highly Efficient Anode Material for Lithium Ion Batteries

Xuejie Gao[§], Jiwei Wang[§], Duo Zhang, Kaiqi Nie, Yanyun Ma, Jun Zhong, Xuhui Sun**

Experimental Section

Synthesis of Fe₂Ni MIL-88 nanorods

Fe₂Ni MIL-88 nanorods were synthesized using a hydrothermal method reported in the literature. In brief, 96 mg of Ni(NO₃)₂·6H₂O, 181.1 mg of FeCl₃·6H₂O and 166.1 mg of 1,4-benzenedicarboxylic acid (H₂bdc) were mixed in 10 mL dimethyl formamide (DMF) under vigorous stirring until the color of solution became transparent brown-yellow. Subsequently, 2 mL of NaOH solution (0.2 M) was added into the mixture with another 15 min stirring, resulting in a brown-yellow suspension. After that, all product of the suspension was transferred into a 50 mL Teflon-lined autoclave and heated at 100°C for 15 h. After the reaction, the yellow product was collected by centrifugation, washed by ethanol for several times and dried at 70°C overnight.

Synthesis of hollow NiFe₂O₄ NSs@CNR

The powder of Fe₂Ni MIL-88 nanorods was loaded into a tube furnace and heated under a 5% H₂/Ar atmosphere at 500°C for 2 h with a ramp of 2°C/min, leading to FeNi alloy encapsulated in carbon nanorod. The hollow NiFe₂O₄ NSs@CNR could be obtained after the further oxidization of FeNi alloy in CNR (denoted as carbon nanorod) in air at 300°C for 3 h with a ramp of 1.5°C/min.

Characterization

The morphology and crystal structure of the as-prepared products were characterized by using scanning electron microscopy (SEM, Zeiss-supra 55 with acceleration voltage of 10kV) and transmission electron microscopy (TEM, FEI Quanta FRG 200F, operating at 200 kV). X-ray diffraction (XRD, Empyrean, Cu K α) was utilized to investigate the crystalline phase of the product. X-ray photoelectrospectroscopy (XPS, Kratos AXIS ULTRADLD) was performed to determine the chemical states of the products. Raman (LabRAMHR800) spectra were recorded to evaluate the carbon structure and the Brunauer-Emmett-Teller (BET) method was employed to determine the specific surface area. Synchrotron based X-ray absorption spectroscopy (XAS) were performed on the beamline 20 A at the Taiwan Light Source (TLS). Thermogravimetric analysis (Switzerland TGA1) was used to determine the carbon content of hollow NiFe₂O₄ NSs@CNR at a heating rate of 10 °C/min in air from room temperature to 750 °C.

Electrochemical measurements

The electrochemical properties of the hollow NiFe₂O₄ NSs@CNR were evaluated by using 2032-type coin cells. The working electrode was prepared by mixing the active materials, super P carbon and polyvinylidene difluoride in a weight ratio of 8:1:1. The result slurry was then coated on Cu foil, and dried at 80°C for 12 h under vacuum. The mass loadings of active materials were about 1.3mg/cm². The cells were assembled in an Ar-filled glove box with Li foil as counter and reference electrodes and porous polypropylene film as the separator, respectively. The electrolyte solution was 1M

LiPF₆ in a mixture of ethylene carbonate (EC), diethyl carbonate (DEC) and dimethyl carbonate (DMC) (1:1:1 by volume). The galvanostatic charge-discharge performance were evaluated with a LAND test system with a voltage range of 0.01-3 V (vs. Li/Li⁺). Cyclic voltammetry was measured between 0.01 and 3 V at a scan rate of 0.1mVs⁻¹. Electrochemical impedance spectroscopy (EIS) was carried out in the frequency range from 100000 to 0.01 Hz with an AC voltage of 5 mV amplitude.

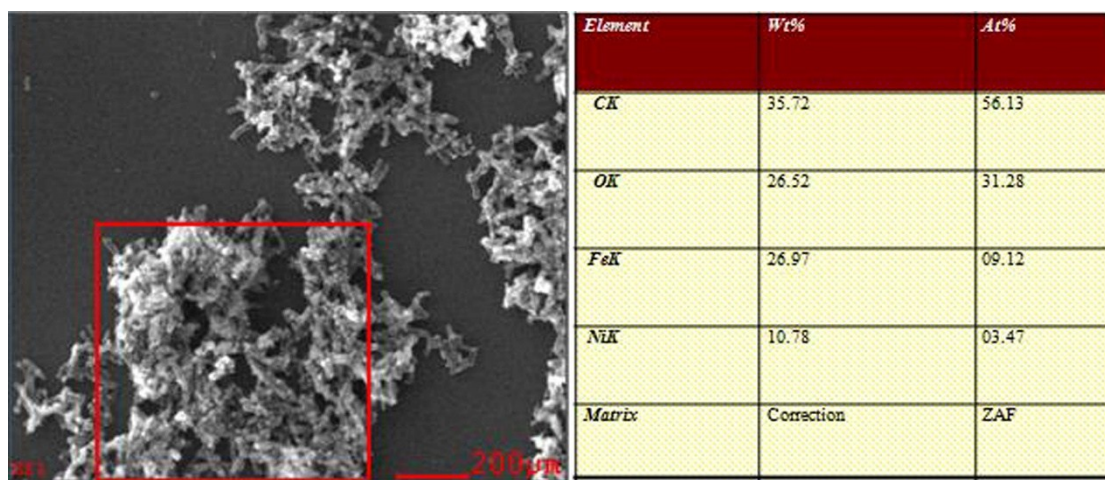


Figure S1. EDX spectrum of NiFe₂O₄ NSs@CNR.

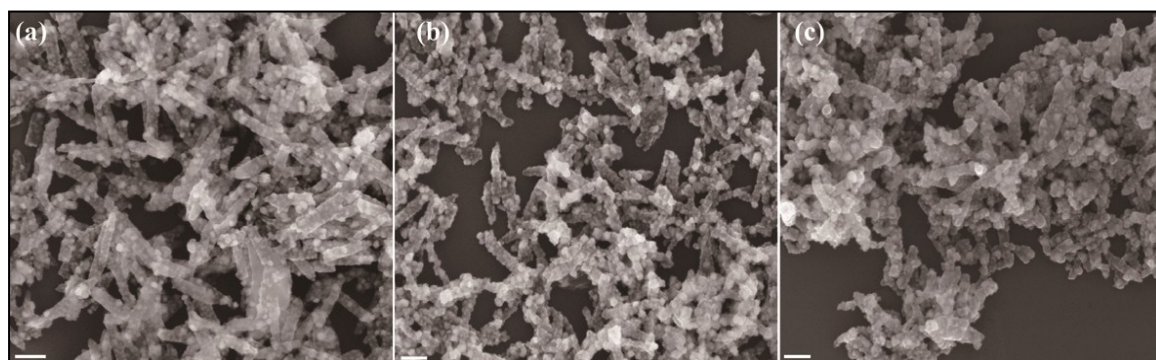


Figure S2. SEM images of product obtained after annealing of FeNi alloy embedded in carbon nanorod at 300 °C for different time: (a) 1h, (b) 2h, and (c) 4h. (Scale bar: 200nm).

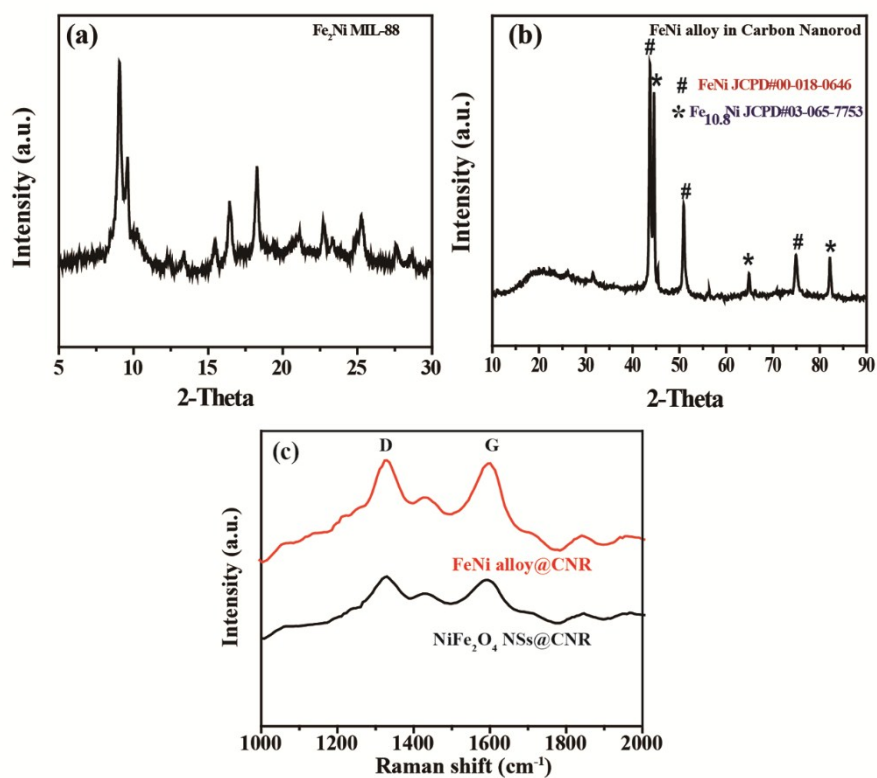


Figure S3. XRD pattern of $\text{Fe}_2\text{Ni MIL-88}$ (a), FeNi alloy in carbon nanorod (b), Raman spectra of FeNi alloy in CNR and NiFe_2O_4 NSs@CNR (c).

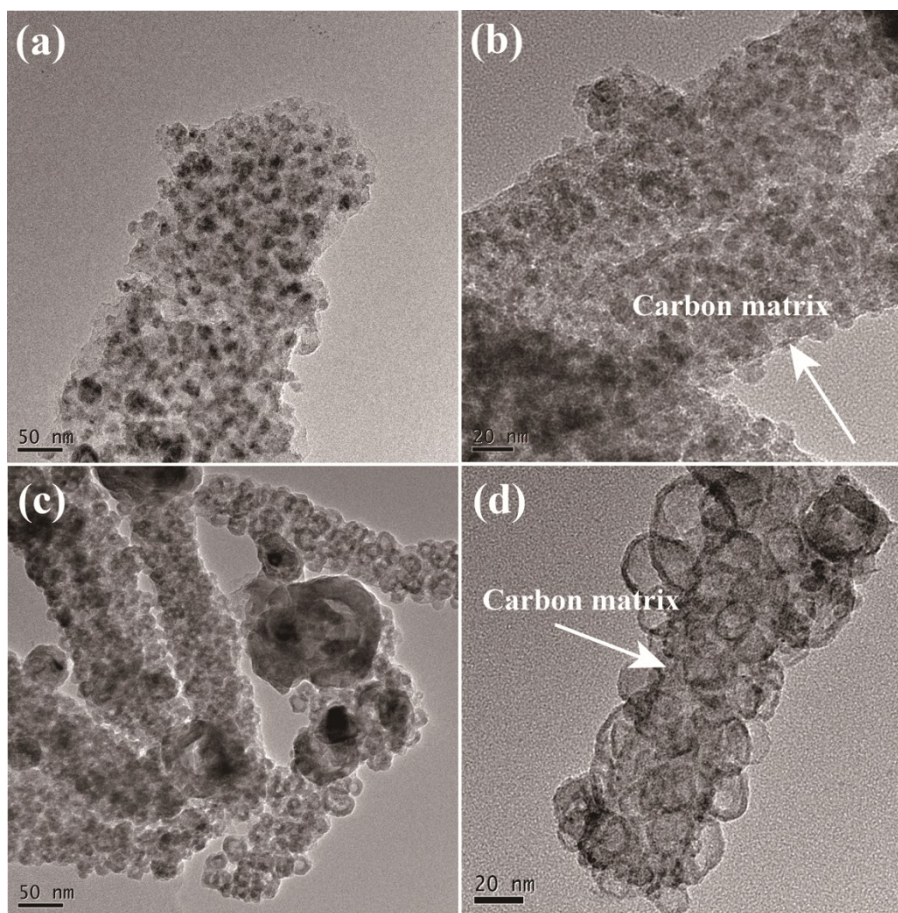


Figure S4. TEM images of FeNi alloy in CNR (a,b) and hollow NiFe₂O₄ NSs@CNR (c,d).

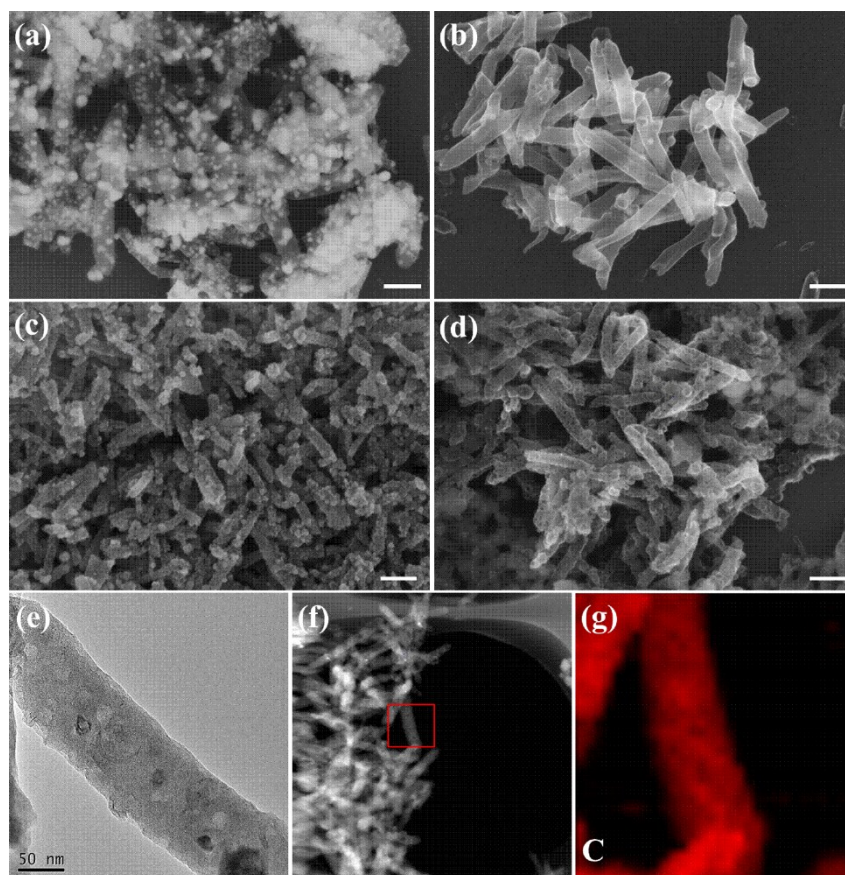


Figure S5 SEM image of FeNi alloy in carbon nanorods before (a) and after acid etching (b), SEM image of NiFe₂O₄ NSs@CNR before (c) and after acid etching (d), respectively. TEM image of NiFe₂O₄ NSs@CNR after acid etching (e), and the corresponding elemental mapping images (f-g).

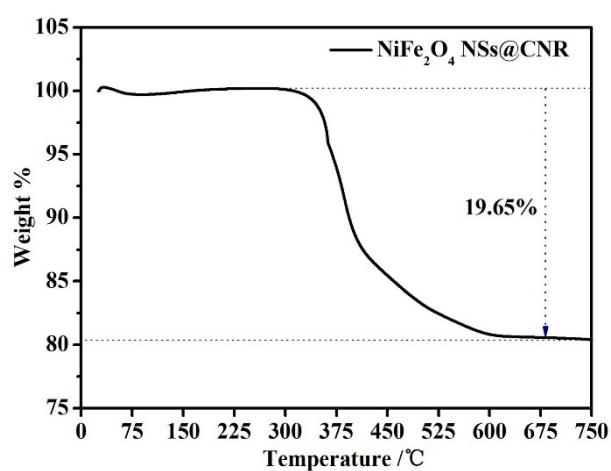


Figure S6. TGA curve of NiFe₂O₄ NSs@CNR

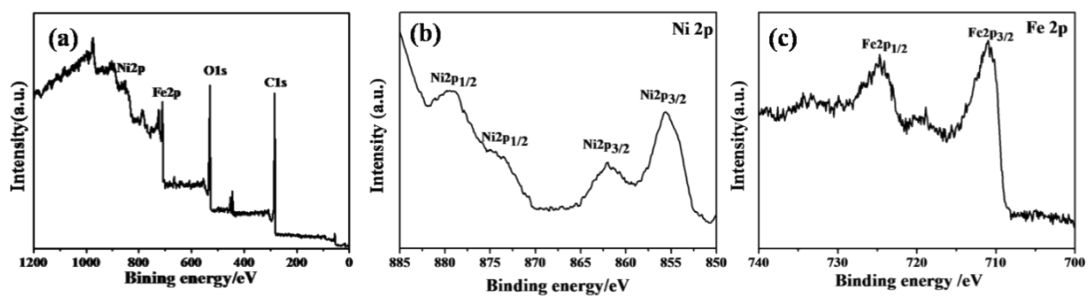


Figure S7. XPS spectra of NiFe₂O₄ NSs@CNR: fully scanned XPS spectrum (a) and high-resolution XPS spectra for (b) Ni 2p, (c) Fe 2p.

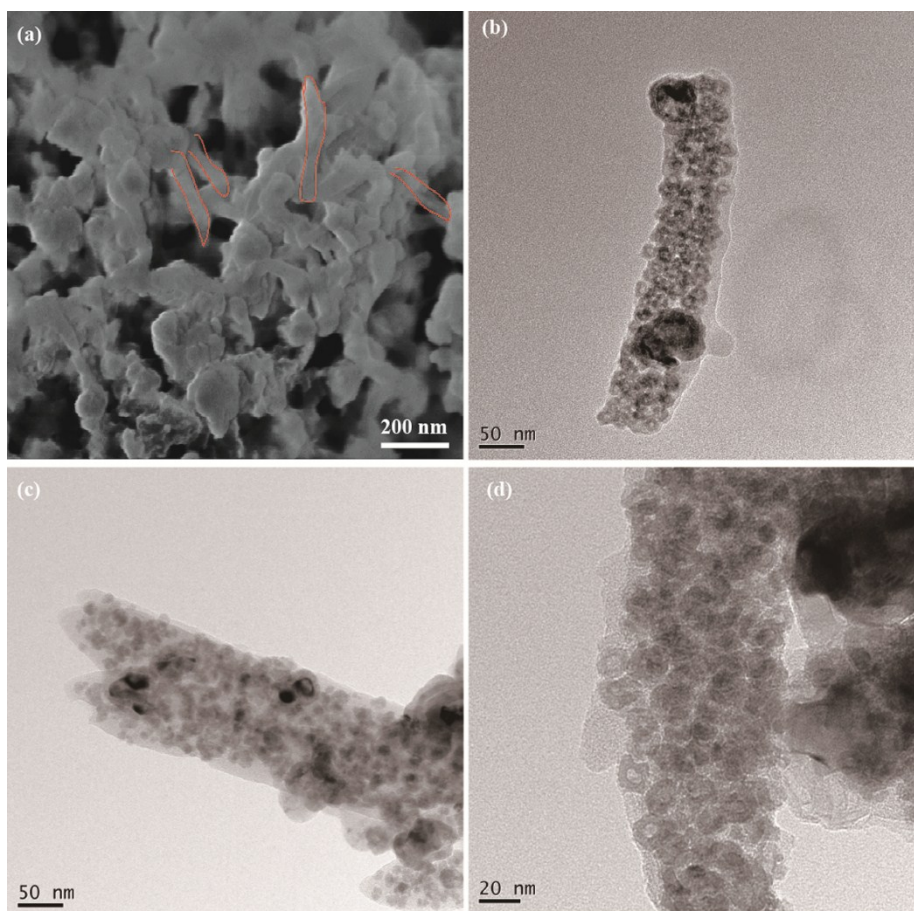


Figure S8. SEM image of the anode (a), TEM images of NiFe₂O₄ NSs@CNR (b-d), after 100 cycles at 0.1 C.

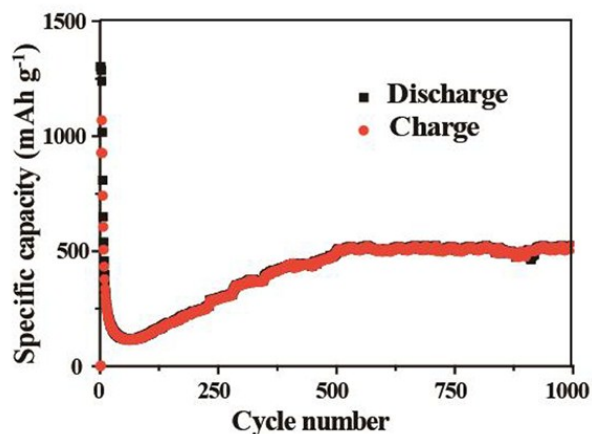


Figure S9. Electrochemical performance of hollow NiFe₂O₄ NSs@CNR at a rate of 2 C after 1000 cycles.

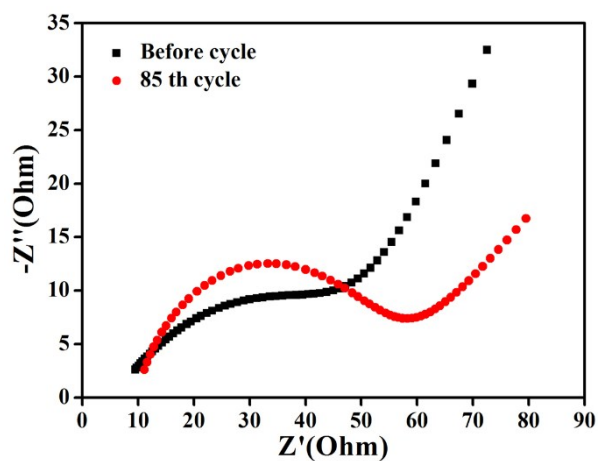


Figure S10. Nyquist plots of cycling (before cycle and 85th cycle) at the rate of 0.1C.

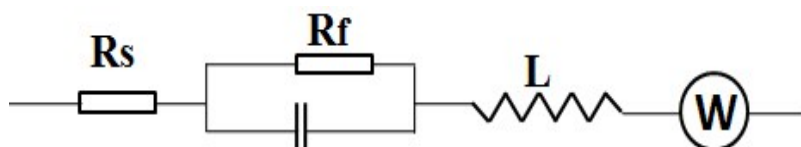


Figure S11. Equivalent circuit for NiFe₂O₄ NSs@CNR electrode/electrolyte interface. R_s is the electrolyte resistance, and R_f and C are the resistance and capacitance of the surface film formed on the electrodes, respectively. L is charge-transfer resistance and W is the Warburg impedance related to the diffusion of lithium ion into the bulk electrodes.

NiFe ₂ O ₄ based anodes	Current density/rate	Cycle number	Specific capacity(mAhg ⁻¹)	Reference
NiFe ₂ O ₄ -C composite	1/8 C	40	780	1
Graphene-NiFe ₂ O ₄ -C sandwich structure	500 mA/g	200	1195	2
Core-shell NiFe ₂ O ₄ @TiO ₂ nanorods	100 mA/g	100	1043	3
NiFe ₂ O ₄ -Fe ₂ O ₃ nanotubes	100 mA/g	100	936.9	4
PDA functionalized graphene-NiFe ₂ O ₄ composite	1A/g	50	838	5
NiFe ₂ O ₄ hollow boxes	1A/g	100	847	6
NiO/NiFe ₂ O ₄ nanoplates -graphene composites	0.1A/g	100	540	7
NiFe ₂ O ₄ nanotubes	100 mA/g	220	1349	8
NiFe ₂ O ₄ NPs within a carbon network	1C	100	381.8	9
Hollow NiFe ₂ O ₄ NSs @CNR	2C(1830mA/g)	1000	513.7	This work
	1C(915mA/g)	400	1045.6	
	0.1 C (91.5 mA/g)	100	1355	

Table S1. Summary of cycling performance for NiFe₂O₄-based anodes in LIBs.

1. Ding Y., Yang Y. and Shao H., *Journal of Power Sources* 2013, **244**, 610-613.
2. Heidari E. K., Zhang B., Sohi M. H., Ataie A. and Kim J.-K., *journal of materials chemistry A* 2014, **2**, 8314-8322.
3. Huang G., Zhang F., Du X., Wang J., Yin D. and Wang L., *Chem.Eur.J.* 2014, **20**, 11214-11219.
4. Huang G., Zhang F., Zhang L., Du X., Wang J. and Wang L., *journal of materials chemistry A* 2014, **2**, 8048-8053.
5. Xiao Y., Zai J., Li X., Gong Y., Li B., Han Q. and Qian X., *Nano Energy* 2014, **6**, 51-58.
6. Yu H., Fan H., Yadian B., Tan H., Liu W., Hng H. H., Huang Y. and Yan Q., *ACS applied materials & interfaces* 2015, **7**, 26751-26757.
7. Du D., Yue W., Fan X., Tang K. and Yang X., *Electrochimica Acta* 2016, **194**, 17-25.

8. Jianan Wang G. Y., * Ling Wang and Wei Yan*, *Journal of materials chemistry A* 2016, **6**, 8620-8629.
9. Preetham P S. M., Shantikumar V. Nair, Dhamodaran Santhanagopalan and Alok Kumar Rai*, *RSC Advances* 2016, **6**, 38064-38070.